Boron-11 and Proton Nuclear Magnetic Resonance Study of *anti*-$B_{18}H_{22}$* and its Anions, *anti*-$[B_{18}H_{21}]^-$ and *anti*-$[B_{18}H_{20}]^{2-}$. The Crystal and Molecular Structure of $[NMe_4]_2$[*anti*-$B_{18}H_{20}$]†

Xavier L. R. Fontaine, Norman N. Greenwood, John D. Kennedy, and Peter MacKinnon
School of Chemistry, University of Leeds, Leeds LS2 9JT

The neutral borane *anti*-$B_{18}H_{22}$ (**1**), and its mono- and di-anions, in $[C_{10}H_6(NMe_2)_2H]$[*anti*-$B_{18}H_{21}$] (**2**) and $[NEt_4]_2$[*anti*-$B_{18}H_{20}$] (**3**) respectively, have been characterized by two-dimensional [^{11}B–^{11}B]-COSY, [^{1}H–^{1}H]-COSY, and ^{1}H-{^{11}B(selective)} n.m.r. spectroscopy, and by [^{1}H–^{11}B] shift correlations. Deprotonation of compound (**1**) is shown to occur with the loss of the bridging hydrogen atoms associated with the *conjuncto*-boron atoms. A single-crystal *X*-ray diffraction analysis of $[NMe_4]_2$ [*anti*-$B_{18}H_{20}$] (**4**) showed the crystals to be monoclinic, space group $P2_1/c$, with a = 693.6(1), b = 1 601.6(3), c =1 131.6(2) pm, β = 102.07(1)°, and Z = 2. The borane anion lies on the crystallographic centre of symmetry and the solid-state structure confirms that obtained from n.m.r. spectroscopy.

A brief description of the n.m.r. behaviour of *anti*-$[B_{18}H_{21}]^-$, that cites some of our preliminary work in this area, has been recently reported.[1] This prompts us to report our more definitive study on this species, which has led to a complete assignment of the boron-11 and proton n.m.r. spectra, and to the unequivocal location of the site of deprotonation. The original detailed description[2] of the preparation of the isomers of $B_{18}H_{22}$ and its anions included only ^{11}B n.m.r. data at very low field (19.3 MHz), and no proton n.m.r. data were reported. Since then the n.m.r. properties of the $B_{18}H_{22}$ isomers have attracted spasmodic attention[3] but the nature of the deprotonated species remains less well defined. The anions *anti*-$[B_{18}H_{21}]^-$ and *anti*-$[B_{18}H_{20}]^{2-}$ are here investigated by boron–boron and proton–proton two-dimensional n.m.r. spectroscopy, by heteronuclear proton–boron double-resonance experiments, and by proton–boron shift correlations. In addition, the structure of the *anti*-$[B_{18}H_{20}]^{2-}$ anion has been determined in the solid state by single-crystal *X*-ray diffraction analysis and is consistent with that obtained in solution by n.m.r. spectroscopy. Comparison of the derived n.m.r. parameters for these species is also made.

The numbering scheme for the neutral parent borane is shown in structure (**I**).

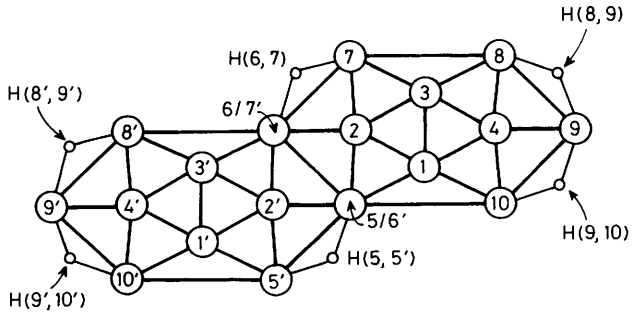

(I)

Results and Discussion

(a) *Boron-11 and Proton N.M.R. Properties of anti*-$B_{18}H_{22}$ (**1**).—The isomers of $B_{18}H_{22}$ have long been known[2] to be strong diprotic acids [equations (1) and (2)]. For both isomers[2]

$$\textit{anti-}\text{ or }\textit{syn-}B_{18}H_{22} + H_2O \longrightarrow \textit{anti-}\text{ or }\textit{syn-}[B_{18}H_{21}]^- + H_3O^+;\ pK_{a_1} \quad (1)$$

$$\textit{anti-}\text{ or }\textit{syn-}[B_{18}H_{21}]^- + H_2O \longrightarrow \textit{anti-}\text{ or }\textit{syn-}[B_{18}H_{20}]^{2-} + H_3O^+;\ pK_{a_2} \quad (2)$$

the first ionization constant, pK_{a_1}, is immeasurably strong and is comparable with those of mineral acids. Values of the second ionization constant, pK_{a_2}, are smaller, being 7.5 and 8.6 for the *anti*- and *syn*-isomers respectively.

Initially,[2] deprotonation of compound (**1**) was thought to occur sequentially at atoms B(9) and B(9′) to give rise to *anti*-$[B_{18}H_{21}]^-$ and *anti*-$[B_{18}H_{20}]^{2-}$ structures in which either of H(8,9) or H(9,10) and then H(8′,9′) or H(9′,10′) were ionized. An ^{11}B n.m.r. examination[2] of the deprotonation of compound (**1**) in base-catalysed deuterium-exchange reactions showed that the most rapid exchange occurred at sites then tentatively assigned to these positions. We here report that two-dimensional [^{11}B-^{11}B]-{^{1}H}-COSY n.m.r. permits the unambiguous assignment of all boron resonances of compound (**1**), so that it is now apparent that the ^{11}B resonance, previously tentatively assigned (at very low operating frequency, 19.3 MHz) to B(9) and B(9′), is most probably due to boron at position B(5) [and its equivalent, by C_i molecular symmetry, at position B(6)]. This suggests that deprotonation occurs at either of these two positions. The 128-MHz ^{11}B and ^{11}B-{^{1}H} n.m.r. spectra of compound (**1**) are shown in Figure 1, together with its [^{11}B–^{11}B]-{^{1}H}-COSY n.m.r. spectrum. Boron and proton n.m.r. assignments and data are summarized in Table 1.

Sufficient cross-peaks were apparent in the [^{11}B–^{11}B]-COSY spectrum to assign it; one additional noteworthy aspect being the observation of (weak) cross-peaks corresponding to couplings between B(5) and B(10) and between B(7) and B(8). These correlations are frequently not observed in other *nido*-

* I.U.P.A.C. recommended nomenclature for *anti*-$B_{18}H_{22}$ is *nido*-decaborano(14)[6′,7′:5,6]-*nido*-decaborane(14), and for *syn*-$B_{18}H_{22}$ is *nido*-decaborano(14)[6′,7′:6,7]-*nido*-decaborane(14).

† Tetramethylammonium *nido*-decaborano[6′,7′:5,6]-*nido*-decaborate(2−).

Supplementary data available: see Instructions for Authors, *J. Chem. Soc., Dalton Trans.*, 1988, Issue 1, pp. xvii—xx.

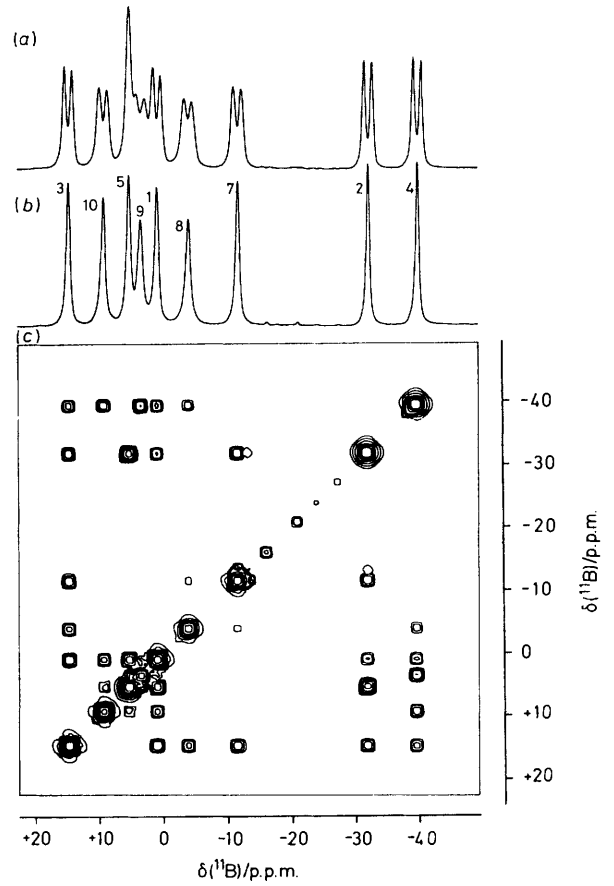

Figure 1. 128-MHz ^{11}B n.m.r. spectra of *anti*-$B_{18}H_{22}$ (**1**) in C_6D_6 solution. (*a*) Straightforward ^{11}B n.m.r. spectrum. (*b*) ^{11}B N.m.r. spectrum recorded under conditions of {^1H(broad-band noise)} decoupling. (*c*) [^{11}B–^{11}B]-COSY contour plot, for which data were also gathered under conditions of {^1H(broad-band noise)} decoupling

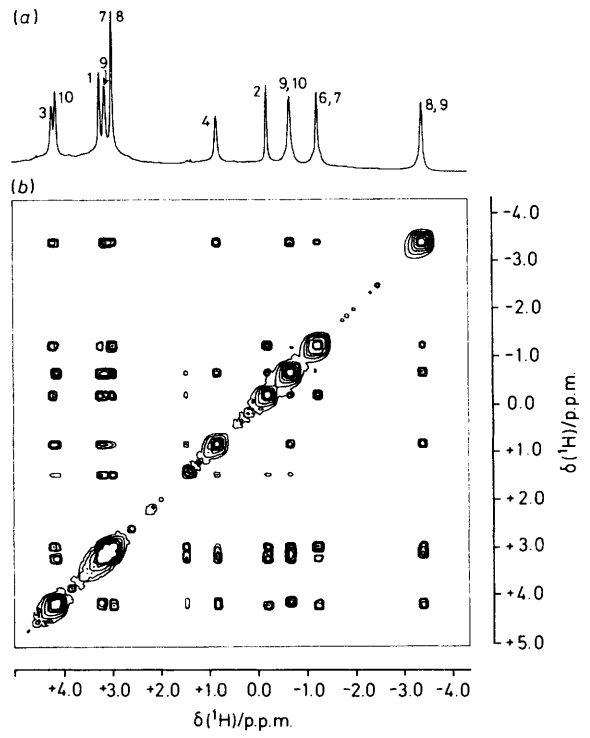

Figure 2. 400-MHz ^1H-{^{11}B(broad-band noise)} n.m.r. spectra of *anti*-$B_{18}H_{22}$ (**1**) in C_6D_6 solution. (*a*) Straightforward one-dimensional spectrum. (*b*) [^1H–^1H]-COSY contour plot. Note that there is fine structure on the $^1H(9)$ resonance in (*a*) (quartet character, splitting *ca.* 9 Hz)

decaboranyl-type compounds, thereby implying constants $^1J(^{11}B–^{11}B)$ for these connectivities that are significantly smaller than the others.[4–7]

Complete assignment of the proton n.m.r. spectrum of compound (**1**) was provided by two-dimensional [^1H–^1H]-{^{11}B}-COSY and ^1H–{^{11}B(selective)} n.m.r. spectroscopy. Proton assignments and connectivity data are given in Table 1 and the ^1H-{^{11}B(broad-band noise)} and two-dimensional [^1H–^1H]-COSY spectra are shown in Figure 2. Proton chemical shift values (Table 1) display a noticeable dependence on the solvent medium with the aromatic-solvent induced shielding (a.s.i.s.) $\Delta\sigma(^1H) = [\delta(^1H)_{CD_2Cl_2} - \delta(^1H)_{C_6D_6}]$ ranging from -0.41 ± 0.10 [H(4)] to $+0.58 \pm 0.10$ [H(8,9)] p.p.m. The differential magnitudes and directions of $\Delta\sigma(^1H)$ show that this shielding anisotropy is not due to concentrative effects alone. The terminal hydrogen aoms H(1), H(3), and H(4), which undergo a shift to lower shielding in hexadeuteriobenzene, are bound to the apical boron atoms of the molecule. However, most of the protons on, or adjacent to, the basal (six-membered open-face) boron atoms of each *nido*-decaboranyl-type subcluster are shifted to higher field; these are H(2′) [equivalent to H(2)], H(8), H(9), and the bridging hydrogen atoms H(6,7), H(8,9), H(9,10). A weak interaction or molecular complex in which the plane of a molecule of hexadeuteriobenzene is lying over the open-face of the subclusters may partially account for these observations (compare ref. 8).

(b) *Boron-11 and Proton N.M.R. Properties of* [$C_{10}H_6(NMe_2)_2H$][*anti*-$B_{18}H_{21}$] (**2**).—Compound (**1**) is readily deprotonated by reaction with a molar equivalent of the weak nucleophile *N,N,N′,N′*-tetramethyl-1,8-diaminonaphthalene ['proton sponge', $C_{10}H_6(NMe_2)_2$] in dichloromethane to give *anti*-$[B_{18}H_{21}]^-$. The ^{11}B–{^1H(broad-band noise)} n.m.r. spectrum shows few coincidences and allows reasonably definitive ^{11}B COSY assignments to the boron framework (Table 2), the assignments being confirmed by [^1H-^1H]-COSY work (see below). Figure 3 shows the ^{11}B, ^{11}B-{^1H}, and [^{11}B–^{11}B]-COSY spectra of compound (**2**) which are essentially in accord with those recently reported[1] for *anti*-$[B_{18}H_{21}]^-$ obtained from the reaction between $[B_9H_{12}]^-$ and CF_3CO_2H in CH_2Cl_2. Observed boron–boron COSY cross-correlations are displayed as solid lines in structure (**II**). One feature of the

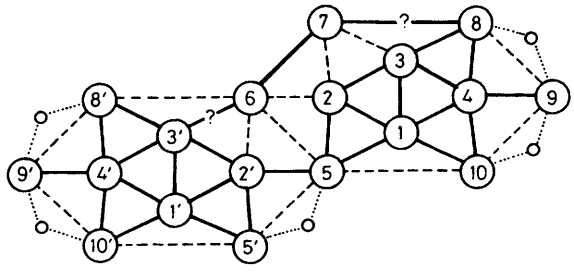

(II)

connectivity data for compound (**2**) contrasts with those of compound (**1**): correlation (albeit weak) between boron atoms B(6) and B(7) [B(5) and B(7) in compound (**1**)] is observed in the anion but not in the neutral borane. On the other hand,

Table 1. Measured n.m.r. properties for *anti*-$B_{18}H_{22}$

Assignment[a]	$\delta(^{11}B)$/p.p.m.[b,c]	Observed two-dimensional [^{11}B–^{11}B]-COSY correlations[d]	$\delta(^{1}H)$/p.p.m.[c,e]	Observed two-dimensional [^{1}H–^{1}H]-COSY correlations[d]	$^{1}J(^{11}B–^{1}H)$/Hz[c,f]
3	+14.6 (+14.7)	1m 2m 4m 7m 8m	+3.87 (+4.19)	1w? 2m 4s 7m[g] 8m[g] 9w?[h] 6,7m 8,9m	150 (149)
10	+9.4 (+9.2)	1w 4m 5w?	+4.07 (+4.12)	1m 4w? 8w?[h] 6,7w 8,9w? 9,10s	161 (153)
5[i]	+5.5 (+5.2)	1m 2s 10w?	—	—	—
9	+3.6 (+3.4)	4m	+3.39 (+3.11)	3w?[h] 4m 6,7w?[h] 8,9m 9,10ms	165 (169)
1	+0.8 (+0.9)	2m 3m 4m 5m 10m	+3.06 (+3.21)	2m 3w? 4m 10m 6,7w[h] 9,10w	150 (148)
8	−4.0 (−4.0)	3m 4w 7vw	+3.01 (+2.95)	3m 4w? 10w?[h] 8,9w[g] 9,10w	160 (148)
7	−11.5 (−11.6)	2m 3m 8vw	+2.97 (+2.96)	2w 3m 6,7ms	162 (156)
2	−31.7 (−31.9)	1m 3m 5s 7m	−0.08 (−0.22)	1m 3m 7w 6,7ms 9,10w?	160 (159)
4	−39.7 (−39.5)	1m 3m 8w 9m 10m	+0.43 (+0.84)	1m 3s 8w? 9m 10w? 8,9m 9,10m	158 (157)
9,10	—	—	−0.38 (−0.71)	1w? 2w? 4m 8w 9ms 10s 6,7w 8,9ms	—
6,7[j]	—	—	−0.89 (−1.27)	1w[k] 2ms 3m 7s 9w?[h] 10w? 8,9w 9,10w[k]	—
8,9	—	—	−2.87 (−3.45)	3m 4m 8w 9m 10w? 6,7w 9,10ms	—

[a] By two-dimensional [^{11}B–^{11}B]- and [^{1}H–^{1}H]-COSY n.m.r. (columns 3 and 5). [b] ±0.05 p.p.m. to high frequency of $BF_3(OEt)_2$. [c] In CD_2Cl_2 solution at 294 K. The values in parentheses are for C_6D_6 solution at 294 K. [d] s = Strong, m = medium, w = weak, v = very. In C_6D_6 solution at 294 K. [e] ±0.05 p.p.m. to high frequency of $SiMe_4$. [f] ±8 Hz; obtained from ^{11}B spectrum with resolution enhancement to achieve baseline separation of doublet components. [g] Because of the overlap of $^{1}H(7)$ and $^{1}H(8)$, the assignments are made on the basis that the most intense correlations are due to $^{3}J(^{1}H–B–B–^{1}H)$. [h] $^{4}J(^{1}H–B–B–B–^{1}H)$. [i] Equivalent to B(6), by C_i molecular symmetry. [j] Equivalent by molecular C_i symmetry to H(5,5′). [k] These assignments arise from correlation to $^{1}H(5',6')$ which is equivalent by symmetry.

Table 2. Measured n.m.r. parameters for *anti*-$[B_{18}H_{21}]^-$[a]

Assignment[b]	$\delta(^{11}B)$/p.p.m.[c,d]	Observed two-dimensional [^{11}B–^{11}B]-COSY correlations[e]	$\delta(^{1}H)$/p.p.m.[d,f,g]	Observed two-dimensional [^{1}H–^{1}H]-COSY correlations[e]	$^{1}J(^{11}B–^{1}H)$/Hz[h]
6	+17.0	3′vw 7w	—	—	—
1′	+13.4	2′ms 3′m 4′m 5′m 10′w	+3.50[i]	2′m 3′m 4′m 5′m 10′m 5,5′m 9′,10′m[j]	142
8′	+9.3	3′m 4′w	+3.73	3′m 4′m 10′w[k] 8′,9′s 9′,10′w	154
3	+5.1	1m 2s 4w 8w	+2.98[l]	1w 2m 4m 7m 8w 8,9w	137
10	+3.2	1m 4m	+3.51[i]	1ms 4m 8m[k] 5,5′m 8,9w 9,10s[j]	140
5	+0.1	1m 2m 2′s	—	—	—
9′	−1.2	4′m	+2.94[l]	4′w 8′,9′s 9′,10′s	*m*
7	−3.4	6w 8vw?	+2.76	2m 3m 8m	137
3′	−4.5	1′m 2′m 4′w 6vw? 8′m	+2.64[n]	1′m 2′m 4′w 8′m 8′,9′m[j]	143
9	−7.7	4m	+2.55	4w 8vw 8,9s 9,10s	155
10′	−10.0	1′w 4′w[o]	+2.44	1′m 4′w 5′w? 8′w[k] 8′,9′w 9′,10′s	~92?[p]
1	−10.6	2m 3m 4m 5m 10m[o]	+2.11	2s 3w 4w 10m 5,5′w, 9,10ms	137
8	−13.0	3m, 4w, 7vw?	+1.86	3w 4w 7ms 9vw 10w[k] 8,9m 9,10w	184 ± 15[q]
5′	−13.6	1′m 2′m	+2.62[n]	1′m 2′m 4′w[k] 10′w? 5,5′s[j]	126 ± 15[q]
2	−24.1	1m 3s 5m	−0.42	1s 3m 7m 5,5′w	145
2′	−29.2	1′m 3′m 5s 5′s	−0.92	1′m 3′m 5′m 5,5′m	150
4′	−39.2	1′m 3′w 8′w 9′m 10′w	+0.17[r]	1′m 3′w 8′w 9′m 10′w 8′,9′w 9′,10′w	150
4	−41.1	1m, 3w 8w, 9m 10m	+0.19[r]	1w 3m 8w 9w 10m 8,9m 9,10w	146
8′,9′	—	—	−1.03	3′m 4′w 8′s 9′s 10′w 9′,10′m	—
9,10	—	—	−1.59	1ms 4w 8w 9s 10s 8,9m	—
5,5′	—	—	−1.88	1w 1′m 2w 2′m 5′s 10m 9′,10′vw?	—
9′,10′	—	—	−3.31	1′m 4′w 8′w 9′s 10′s 5,5′vw? 8′,9′m	—
8,9	—	—	−3.90	3w 4m 8m 9s 10w 9,10m	—

[a] $[C_{10}H_6(NMe_2)_2H]^+$ salt. [b] By [^{11}B–^{11}B]- and [^{1}H–^{1}H]-COSY n.m.r. (columns 3 and 5). [c] ±0.5 p.p.m. to high frequency of $BF_3(OEt)_2$. [d] In CD_2Cl_2 solution at 294 K. [e] s = Strong, m = medium, w = weak, v = very. [f] ±0.05 p.p.m. to high frequency of $SiMe_4$. [g] Additional resonances due to the $[C_{10}H_6(NMe_2)_2H]^+$ cation at $\delta(^{1}H)$/p.p.m. 8.06—7.96 and 7.77—7.59 (aromatic); 3.18 [s, $(CH_3)_2N$]. [h] ±8 Hz (unless otherwise stated); from ^{11}B spectrum with resolution enhancement to achieve baseline separation of doublet components. [i] Assignment from two-dimensional [^{11}B–^{1}H]-COSY n.m.r. which shows B(1′)–H(1′)m, and B(10)–H(10)m. [j] Assignments assume $^{3}J(^{1}H–B–B–^{1}H)$ is the most intense and is the only one observed. [k] $^{4}J(^{1}H–B–B–B–^{1}H)$. [l] Assignment from two-dimensional [^{11}B–^{1}H]-COSY n.m.r., B(3)–H(3)m, B(9′)–H(9′)w. [m] Not sufficiently resolved from B(7) resonance for measurements. [n] Assignment from two-dimensional [^{11}B–^{1}H]-COSY n.m.r., B(3′)–H(3′)m, B(5′)–H(5′)w. [o] Due to overlap of B(10′) and B(1) resonances, the assignments assume only $^{1}J(^{11}B–^{11}B)$ is observed. [p] Estimate; there is doublet overlap of B(1) with B(10′). [q] Doublets due to B(5′) and B(8) overlapped and were not sufficiently well resolved for more accurate measurement. [r] Assignment from [^{11}B–^{1}H]-COSY n.m.r., B(4)–H(4)s, B(4′)–H(4′)s.

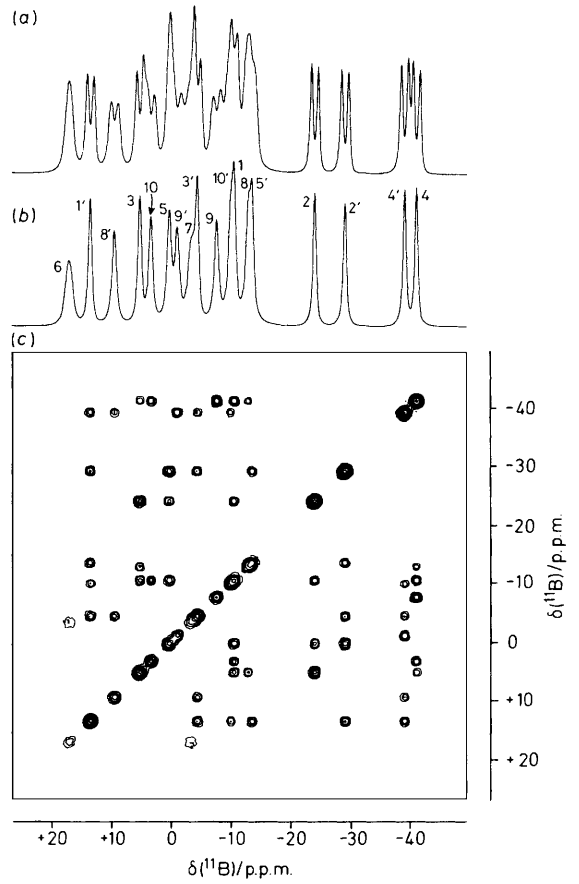

Figure 3. 128-MHz ^{11}B n.m.r. spectra of $[C_{10}H_6(NMe_2)_2H][anti\text{-}B_{18}H_{21}]$ (**2**) in CD_2Cl_2 solution. (*a*) Straightforward ^{11}B n.m.r. spectrum. (*b*) ^{11}B n.m.r. spectrum recorded under conditions of $\{^1H$(broad-band noise)$\}$ decoupling. (*c*) $[^{11}B$–$^{11}B]$-COSY contour plot, for which data were also gathered under conditions of $\{^1H$(broad-band noise)$\}$ decoupling

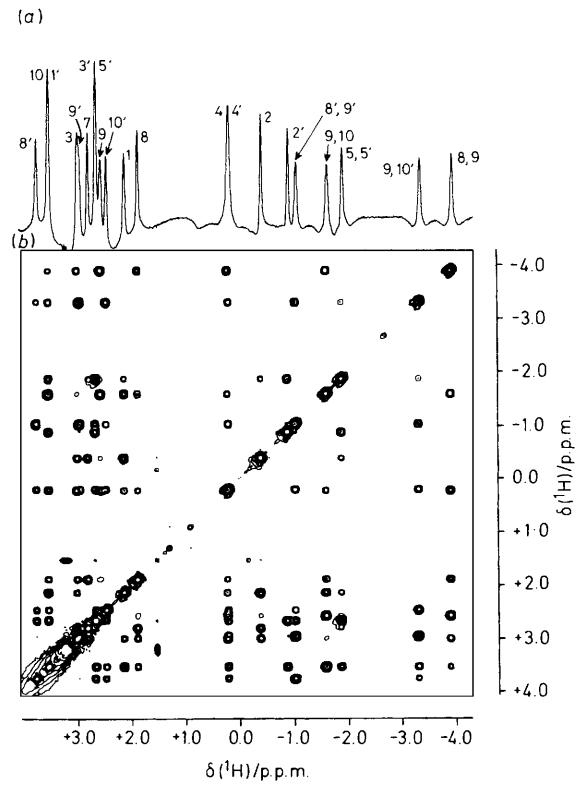

Figure 4. 400-MHz $^1H\{^{11}B$(broad-band noise)$\}$ n.m.r. spectra of $[C_{10}H_6(NMe_2)_2H][anti\text{-}B_{18}H_{21}]$ (**2**) in CD_2Cl_2 solution. (*a*) Conventional one-dimensional spectrum from which an otherwise equivalent $^1H\text{-}\{^{11}B$(broad-band noise; off-resonance)$\}$ trace has been subtracted. (*b*) The corresponding section of the $[^1H$–$^1H]$-COSY contour plot

correlations between B(5) and B(5′); B(8) and B(9); B(9) and B(10); B(8′) and B(9′); and B(9′) and B(10′) are not observed, nor are the corresponding correlations for compound (**1**), *viz.* B(5)–B(7), B(8)–B(9), and B(9)–B(10), all consistent with weak interboron couplings associated with B–H–B bonds, as also observed in other *nido*-decaboranyl-type species.[4–7] The observed $[^{11}B(6)$–$^{11}B(7)]$ correlation in compound (**2**) is thereby of interest, and is consistent with greater *s*-electron density and overlap involved in the B(6)–B(7) interaction and hence, more localized two-electron two-centre bonding in this linkage. Thus, observation of an $^{11}B(6)$–$^{11}B(7)$ correlation albeit of weak intensity, strongly suggests that deprotonation occurs by loss of the bridging proton at this position, *viz.* $^1H(6,7)$.

Two-dimensional $[^1H$–$^1H]$-COSY n.m.r. spectroscopy is proving an important tool in polyhedral boron and metallaborane chemistry.[9] The two-dimensional $[^1H$–$^1H]$-COSY n.m.r. spectrum of $[C_{10}H_6(NMe_2)_2H][anti\text{-}B_{18}H_{21}]$ (4.0 to −4.5 p.p.m.) is shown in Figure 4 together with a one-dimensional spectrum from which an equivalent $^1H\text{-}\{^{11}B$-(broad-band noise; off resonance)$\}$ spectrum has been subtracted. Connectivity information derived from two-dimensional $[^{11}B$–$^{11}B]$-, $[^1H$–$^1H]$-COSY, and $^1H\text{-}\{^{11}B$-(selective)$\}$ n.m.r. spectroscopy and two-dimensional $[^1H$–$^{11}B]$ shift correlation methods is given in Table 2. Correlations to bridging hydrogen atoms are important since they provide information not available from $[^{11}B$–$^{11}B]$-COSY n.m.r. spectroscopy.[9] Correlations to the bridging hydrogen atoms of compound (**2**) are displayed as solid lines in structure (**III**). It is

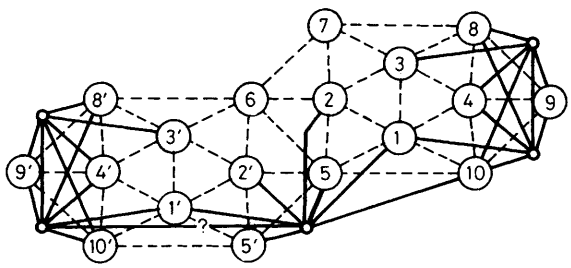

(III)

readily apparent from the assignment of the bridging hydrogen atoms of compound (**2**) that deprotonation occurs with the removal of a proton from the B(7) and *conjuncto*-B(6) B–H–B position, this being in agreement with information provided by the $[^{11}B$–$^{11}B]$-COSY spectrum and with the previous observations[2] of deuterium-exchange reactions as discussed above.

There are a large number of correlations to bridging hydrogen atoms [structure (**III**)]: ^1H(bridge)-^1H(bridge) cross-peaks locate the positions of these atoms relative to one another, $^2J[^1H$(bridge)–^1H(terminal)$]$ cross-peaks locate the positions of bridging hydrogen atoms to the basally bound terminal hydrogen atoms, and $^3J[^1H$(bridge)–^1H(terminal)$]$ cross-peaks relate the hydrogen atoms of apical boron atoms to their bridging counterparts. Together these correlations provide

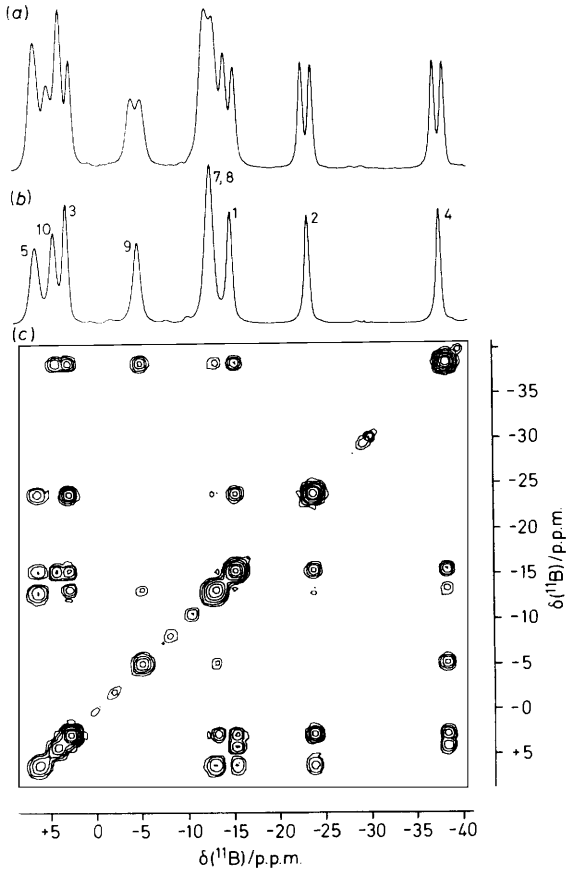

Figure 5. 128-MHz ^{11}B n.m.r. spectra of $[NEt_4]_2[anti\text{-}B_{18}H_{20}]$ (**3**) in $(CD_3)_2CO$ solution. (*a*) Straightforward ^{11}B n.m.r. spectrum. (*b*) ^{11}B n.m.r. spectrum recorded under conditions of $\{^1H$(broad-band noise)$\}$ decoupling. (*c*) [^{11}B–^{11}B]-COSY contour plot, for which data were also gathered under conditions of $\{^1H$(broad-band noise)$\}$ decoupling

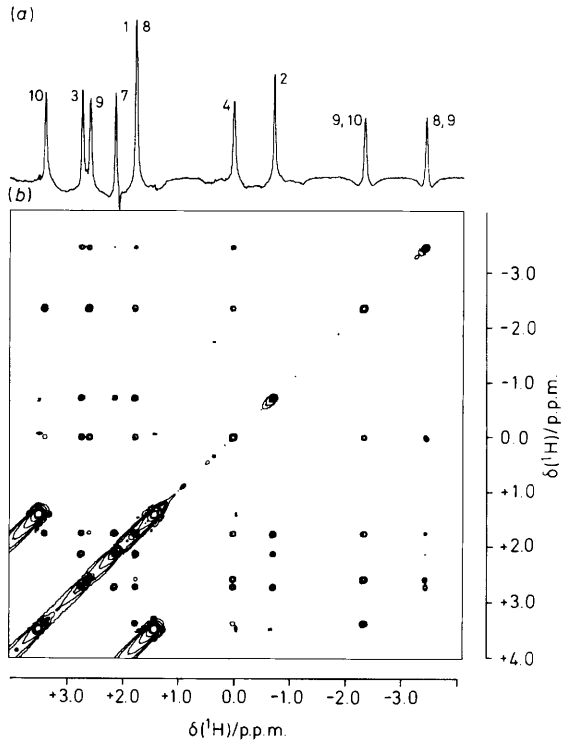

Figure 6. 400-MHz ^1H-$\{^{11}B$(broad-band noise)$\}$ n.m.r. spectra of $[NEt_4]_2[anti\text{-}B_{18}H_{20}]$ (**3**) in $(CD_3)_2CO$ solution. (*a*) Conventional one-dimensional spectrum from which an otherwise equivalent ^1H-$\{^{11}B$(broad-band noise; off-resonance)$\}$ trace has been subtracted. (*b*) The corresponding section of the [^1H–^1H]-COSY contour plot

sufficient evidence to assign the bridging hydrogen locations in compound (**2**), and thence with the other [^1H–^1H]-COSY data confirm all the ^{11}B and ^1H positional assignments given in Table 2.

Noticeable in the ^1H(bridging)–^1H(terminal) correlations are the vicinal $^3J(^1H$–$^1H)$ cross-peaks between H(4′) and H(8′,9′), and H(9′,10′) [structure (**III**)], which are also mirrored by corresponding couplings between H(4) and H(8,9) or H(9,10) in the deprotonated subcluster.

(c) *Boron-11 and Proton N.M.R. Properties of* $[NEt_4]_2$-$[anti\text{-}B_{18}H_{20}]$ (**3**).—The removal of a second bridging proton from compound (**1**) requires quite basic conditions [as indicated by equation (2), above] and is achieved[2] by reaction of compound (**1**) with ethanolic hydroxide solution followed by treatment with a quaternary ammonium salt. The ^{11}B-$\{^1H\}$ n.m.r. spectrum of the tetraethylammonium salt, together with the two-dimensional [^{11}B-^{11}B]-COSY spectrum are shown in Figure 5. These spectra are greatly simplified compared to those of $anti\text{-}[B_{18}H_{21}]^-$ and suggest a return to the C_i symmetry of compound (**1**). Correspondingly, the ^1H-$\{^{11}B\}$ spectrum (Figure 6) also suggests similar symmetry and displays only two resonances (in the ratio of 2:2) attributable to bridging hydrogen atoms, confirming the loss of two bridging hydrogen atoms from compound (**1**). N.m.r. assignments and data are summarized in Table 3.

The boron cluster framework connectivity provided by the $^1J(^{11}B$–$^{11}B)$-COSY correlations (Table 3) is displayed as solid lines in structure (**IV**). These correlations are observed for most adjacent boron atoms, most noticeably between boron atom types B(5) and B(7). This latter corresponds to correlations between B(5′) and *conjuncto*-B(5), and between B(7) and *conjuncto*-B(6), indicating that deprotonation has occurred by loss of the two bridging protons associated with the edge-fused boron positions.

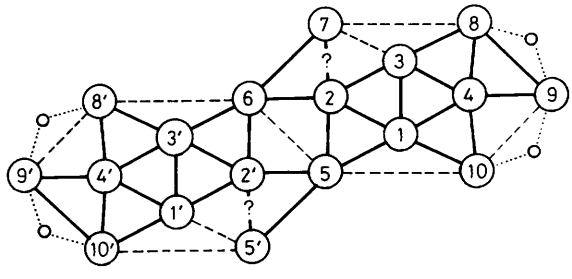

(IV)

[^1H–^1H]-COSY correlations to the bridging hydrogen atoms of compound (**3**) are shown in structure (**V**). These bridging hydrogen atoms show geminal $^2J[^1H$–$^1H]$ correlations to basal hydrogen sites, and vicinal $^3J[^1H$–$^1H]$ correlations to apical boron-bound hydrogen atoms (Figure 6), thus pinpointing the positions of these bridging atoms. It is interesting to note that the correlation between the bridging protons is very weak and that H(8,9) also displays very weak correlations to H(2) and H(7).

(d) *X-Ray Diffraction Analysis of* $[NMe_4]_2anti\text{-}[B_{18}H_{20}]$ (**4**).—Compound (**4**) crystallizes in the centrosymmetric space

Table 3. Measured n.m.r. parameters for $[NEt_4]_2[anti\text{-}B_{18}H_{20}]$

Assignment[a]	$\delta(^{11}B)$/p.p.m.[b,c]	Observed two-dimensional [^{11}B–^{11}B]-COSY correlations[d]	$\delta(^1H)$/p.p.m.[c,e,f]	Observed two-dimensional [^1H–^1H]-COSY correlations[d]	$^1J(^{11}B–^1H)$/Hz[g]
5[h]	+6.1	1m 2m 7s[i]	—	—	—
10	+4.1	1m 4s	+3.38	1ms 4w 9,10s	(181)
3	+2.8	1m 2s 4s 8m	+2.72	1m 2ms 4ms 7s 8m 8,9w	(136)
9	−5.0	4s 8w	+2.58	4ms 8w 8,9w 9,10s	146
7	*ca.* −13.0	2vw? 5s[i,j]	+2.13	2m 3s 8s 8,9vw?	(123)
8	*ca.* −13.0	3m 4w 9w[j]	+1.73	3m 4m 7s 9w 8,9m 9,10m[k]	(123)
1	−15.2	2m 3m 4m 5m 10m	+1.75	2s 3m 4m 10ms 9,10m[k]	134
2	−23.5	1m 3s 5m 7vw?	−0.72	1s 3ms 7m 8,9vw?[l]	138
4	−37.1	1m 3s 8w 9s 10s	0.00	1m 3ms 8m 9ms 10w 8,9m 9,10m	138
9,10	—	—	−2.35	1m 4m 8m 9s 10s 8,9vw?	—
8,9	—	—	−3.46	2vw?[l] 3w 4m 7vw? 8m 9w 9,10vw?	—

[a] By two-dimensional [^{11}B–^{11}B]- and [^1H–^1H]-COSY n.m.r. (columns 3 and 5). [b] ±0.5 p.p.m. to high frequency of $BF_3(OEt)_2$. [c] In $(CD_3)_2CO$ solution at 294 K. [d] s = Strong, m = medium, w = weak, v = very. [e] ±0.05 p.p.m. to high frequency of $SiMe_4$. [f] Additional resonances for the $[NEt_4]^+$ cation; $\delta(^1H)$/p.p.m., 1.41 [br t, $(CH_3CH_2)_4N$], 3.49 (br q, $(CH_3CH_2)_4N$]. Very strong correlation between the two resonances is observed in the two-dimensional [^1H–^1H]-COSY n.m.r. spectrum. [g] ±8 Hz; from ^{11}B spectrum with resolution enhancement to achieve baseline separation of doublet components; values in parentheses indicate an uncertainty in the accuracy of the measurement due to partial overlap of resonances. [h] Equivalent to B(6) by C_i symmetry. [i] Correlation to equivalent boron B(6). [j] There is a near-coincidence of the B(7) and B(8) resonance assignments; it is here assumed only $^1J(^{11}B–^{11}B)$ is observed; there is some distinction in the two-dimensional COSY plot (Figure 6). [k] There is overlap of H(2) and H(4) resonances; the assignments assume $^3J(^1H–B–B–^1H)$ is the most intense and is the only one observed. [l] $^4J(^1H–B–B–B–^1H)$.

Table 4. Selected bond lengths (pm) and angles (°) for $[NMe_4]_2[anti\text{-}B_{18}H_{20}]$, with e.s.d.s in parentheses*

(*i*) Boron–boron

B(1)–B(2)	177.7(5)	B(1)–B(3)	181.0(5)	B(1)–B(4)	181.3(5)
B(1)–B(5)	178.6(5)	B(1)–B(10)	171.3(5)	B(2)–B(3)	173.0(5)
B(2)–B(5)	178.1(5)	B(2)–B(5′)	177.9(5)	B(2)–B(7)	180.1(5)
B(3)–B(4)	180.0(5)	B(3)–B(7)	174.4(5)	B(3)–B(8)	178.1(5)
B(4)–B(8)	180.2(5)	B(4)–B(9)	169.6(6)	B(4)–B(10)	174.5(5)
B(5)–B(2′)	179.9(5)	B(5)–B(10)	210.3(5)	B(5)–B(5′)	179.9(5)
B(5)–B(7′)	167.1(5)	B(7)–B(5′)	167.1(5)	B(7)–B(8)	184.2(5)
B(8)–B(9)	180.0(5)	B(9)–B(10)	175.8(5)		

(*ii*) Boron–hydrogen

B(1)–H(1)	110.8(18)	B(2)–H(2)	109.0(17)	B(3)–H(3)	110.7(18)
B(4)–H(4)	109.6(18)	B(7)–H(7)	1128.(16)	B(8)–H(8)	111.1(16)
B(9)–H(9)	106.5(21)	B(10)–H(10)	112.2(16)	B(8)–H(8,9)	123.8(19)
B(9)–H(8,9)	128.0(18)	B(9)–H(9,10)	126.3(17)	B(10)–H(9,10)	124.1(17)

(*iii*) Angles

B(1)–B(2)–B(3)	62.2(2)	B(8)–B(4)–B(9)	61.8(2)	B(5′)–B(5)–B(10)	113.4(2)
B(3)–B(4)–B(1)	60.3(2)	B(10)–B(5)–B(7′)	115.8(2)	B(5)–B(2)–B(5′)	60.7(2)
B(1)–B(3)–B(2)	60.2(2)	B(2′)–B(5)–B(7′)	62.8(2)	B(7)–B(3)–B(8)	63.0(2)
B(7)–B(8)–B(9)	123.4(2)	B(2)–B(3)–B(4)	114.3(2)	B(9)–B(4)–B(10)	61.4(2)
B(9)–B(10)–B(5)	111.6(2)	B(2)–B(1)–B(4)	111.4(2)	B(5′)–B(5)–B(7)	108.2(2)
B(5)–B(1)–B(10)	73.9(2)	B(1)–B(3)–B(4)	60.3(2)	B(2′)–B(5)–B(10)	100.2(2)
B(5′)–B(2)–B(7)	57.7(2)	B(8)–B(9)–B(10)	104.1(3)		

* Primed atoms refer to those at symmetry position $-x, -y, -z$. The $[NMe_4]^+$ cation is a tetrahedron with N–C = 149.3 pm and C–H = 99.1—99.9 pm.

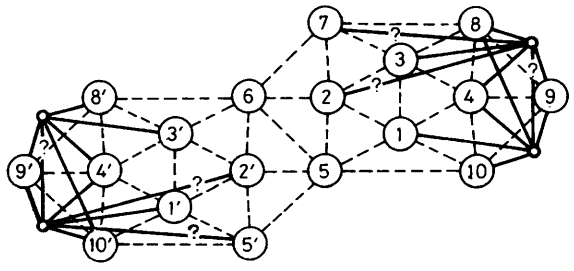

(V)

group $P2_1/c$ with two molecules in the unit cell. The centre of the borane dianion is located on the crystallographic inversion centre, imparting C_i symmetry to the cluster. The unique boron atoms B(1)—B(5) and B(7)—B(10), comprise one *nido*-decaboranyl-type subcluster conjoined at the common B(5)–B(5′).* The structure of the dianion is displayed in Figure 7, and selected dimensions are given in Table 4.

Comparison of interboron distances in compound (**4**) with those obtained for compound (**1**) in earlier studies[10,11] is

* In the crystallographic numbering scheme B(5′) corresponds to B(6) in Figure 7.

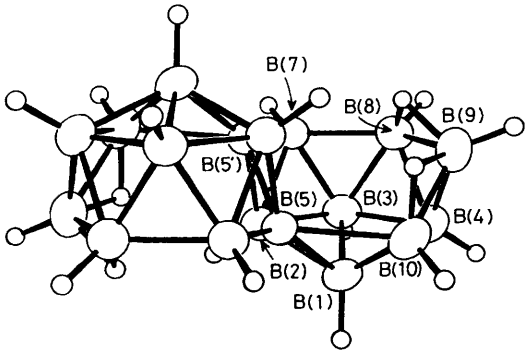

Figure 7. The crystallographically determined structure of the *anti*-$[B_{18}H_{20}]^{2-}$ anion in $[NMe_4]_2[anti\text{-}B_{18}H_{20}]$ (**4**). The primed atoms are related to unprimed atoms by the crystallographic centre of symmetry on the B(5)–B(5′) vector. Thus, for I.U.P.A.C.-recommended nomenclature *conjuncto*-boron atoms B(5) and B(5′) are B(5)/(6′) and B(6)/(7′) respectively

noteworthy. The B(5)–B(10) and B(7)–B(8) distances in compound (**1**) are almost identical at 197.6(4) and 196.8(4) pm. However, in compound (**4**) (Table 4) these are lengthened and shortened to 210.3(5) and 184.2(5) pm respectively; the distance of 210.3(5) pm being very 'long' for a formally bound B–B distance. By contrast, the interboron distance between the *conjuncto*-boron atoms, B(5) and B(5′), is relatively unchanged on removal of the bridging hydrogen atoms attached to both these atoms, *i.e.* 183.8(5) pm in compound (**1**) and 179.9(5) in compound (**4**), suggesting little change in the *conjuncto* linkage on double deprotonation. The other interboron distances show little significant change from those of compound (**1**).

All hydrogen atoms, bridging and terminal, were located in the analysis and thereby confirm the *anti*-$[B_{18}H_{20}]^{2-}$ anionic structure obtained by n.m.r. techniques for compound (**3**) (above). The poor accuracy of boron–hydrogen distances in the earlier determination of the structure of compound (**1**) precludes detailed comparison of these distances with the present values; however, there appear to be no significant differences between the two compounds.

Thus, the only significant geometrical changes on formation of *anti*-$[B_{18}H_{20}]^{2-}$ (**4**) from *anti*-$B_{18}H_{22}$ (**1**) are changes in the B(5)–B(10) and B(7)–B(8) interboron distances. Since these distances are generally [12] long in *nido*-decaboranyl-type systems the resulting perturbation of bonding in the boron cage framework may be very slight. Fractional atomic co-ordinates are given in Table 5.

(e) *Additional N.M.R. Considerations.*—For compounds (**1**), (**2**), and (**3**) a plot of $\delta(^1H)$ *versus* $\delta(^{11}B)$ for directly bound atoms is given in Figure 8(*a*). For the terminal hydrogen atoms there is an overall correlation with a slope of $\delta(^1H):\delta(^{11}B)$ of approximately 1:10. The terminal hydrogen atoms of H(2), H(2′), H(4), and H(4′) display the maximum deviation from these lines of best fit by up to *ca.* 1.6 p.p.m. Although deviations of this magnitude may be expected from local anisotropy variations, *etc.*, the deviations for the H(2), H(2′), H(4), and H(4′) appear to increase with increasing charge on the molecule. The deviations for H(2) and H(2′) each probably arise from its position over the open face of the other subcluster. The increasing use of deviations such as these as a useful structural diagnostic in closely related structural types has recently been noted elsewhere.[13–15]

Comparison of ^{11}B chemical shift data for compounds (**1**)–(**3**) is shown in Figure 8(*b*). Centrosymmetric pairs of boron atoms are linked by dashed lines. It is apparent that there is a general shift to higher shielding for boron atoms other than B(2) and B(4) on going from neutral *anti*-$B_{18}H_{22}$ to *anti*-$[B_{18}H_{20}]^{2-}$, perhaps consistent with increasing shielding from the increasing negative charge. For *anti*-$[B_{18}H_{21}]^-$, resonances corresponding to the deprotonated *nido*-decaboranyl subcluster (labelled with unprimed atom numbers) generally experience a greater shielding than their counterparts in the other subcluster. The exceptions to this are B(6) and B(7) which are dramatically shifted to low field, and since deprotonation has been shown to result in the loss of the H(6,7) bridging proton at this position, the potential diagnostic value of $\delta(^{11}B)$ comparisons such as these in asymmetric *conjuncto*-polyhedra is evident. The bridging hydrogen $\delta(^1H)$ shielding properties also vary markedly over the series (Figure 9), with a general high-field shift with increasing charge again being noteworthy. The exception is H(8,9) which is shifted to marginally lower shielding in compound (**3**). However, the effect is small and may not be significant.

Table 5. Fractional atom co-ordinates ($\times 10^4$) for $[NMe_4]_2[B_{18}H_{20}]$

Atom	*X/a*	*Y/b*	*Z/c*
B(1)	2 233(3)	−458(1)	1 582(2)
B(2)	2 090(3)	339(1)	474(2)
B(3)	2 838(3)	641(1)	1 968(2)
B(4)	1 391(4)	−85(11)	2 899(2)
B(5)	427(3)	−571(1)	205(2)
B(7)	621(3)	1 167(1)	903(2)
B(8)	88(3)	862(1)	2 372(2)
B(9)	−1 109(4)	−101(1)	2 614(2)
B(10)	158(4)	−865(1)	1 957(2)
N	4 758(1)	7 205(1)	7(1)
C(1)	5 831(1)	6 508(1)	−451(1)
C(2)	3 051(1)	6 861(1)	464(1)
C(3)	6 123(1)	7 644(1)	1 010(1)
C(4)	4 028(1)	7 806(1)	−994(1)
H(1)	3 513(26)	−887(10)	1 719(14)
H(2)	3 313(24)	412(9)	14(13)
H(3)	3 754(26)	951(9)	2 442(15)
H(4)	2 213(25)	−193(9)	3 824(16)
H(7)	887(22)	1 854(10)	780(13)
H(8)	−132(23)	1 367(9)	3 002(14)
H(9)	−2 033(28)	−211(10)	3 241(17)
H(10)	35(23)	−1 545(10)	2 168(14)
H(8,9)	−1 552(27)	552(10)	1 962(16)
H(9,10)	−1 544(25)	−581(9)	1 711(15)
H(11)	4 895(1)	6 210(1)	−1 100(1)
H(12)	6 975(1)	6 745(1)	−744(1)
H(13)	6 236(1)	6 113(1)	237(1)
H(21)	3 495(1)	6 451(1)	1 124(1)
H(22)	2 121(1)	6 579(1)	−212(1)
H(23)	2 360(1)	7 343(1)	748(1)
H(31)	5 381(1)	8 114(1)	1 280(1)
H(32)	6 581(1)	7 213(1)	1 643(1)
H(33)	7 251(1)	7 843(1)	661(1)
H(41)	5 195(1)	7 989(1)	−1 302(1)
H(42)	3 198(1)	7 451(1)	−1 624(1)
H(43)	3 313(1)	8 263(1)	−670(1)

Experimental

General.—*nido*-Decaborano(14)[6′,7′:5,6]-*nido*-decaborane(14) (*anti*-$B_{18}H_{22}$) was prepared by the oxidation of $[NMe_4][nido\text{-}B_9H_{12}]$ with HgI_2 according to the reported method.[16] The salts $[NR_4]_2[B_{18}H_{20}]$ (R = Me or Et) were thence prepared according to the literature methods.[2]

Nuclear Magnetic Resonance Spectroscopy.—This was performed at 2.35 and/or 9.40 Tesla on JEOL FX 100 and Bruker AM 400 instruments respectively. The techniques of

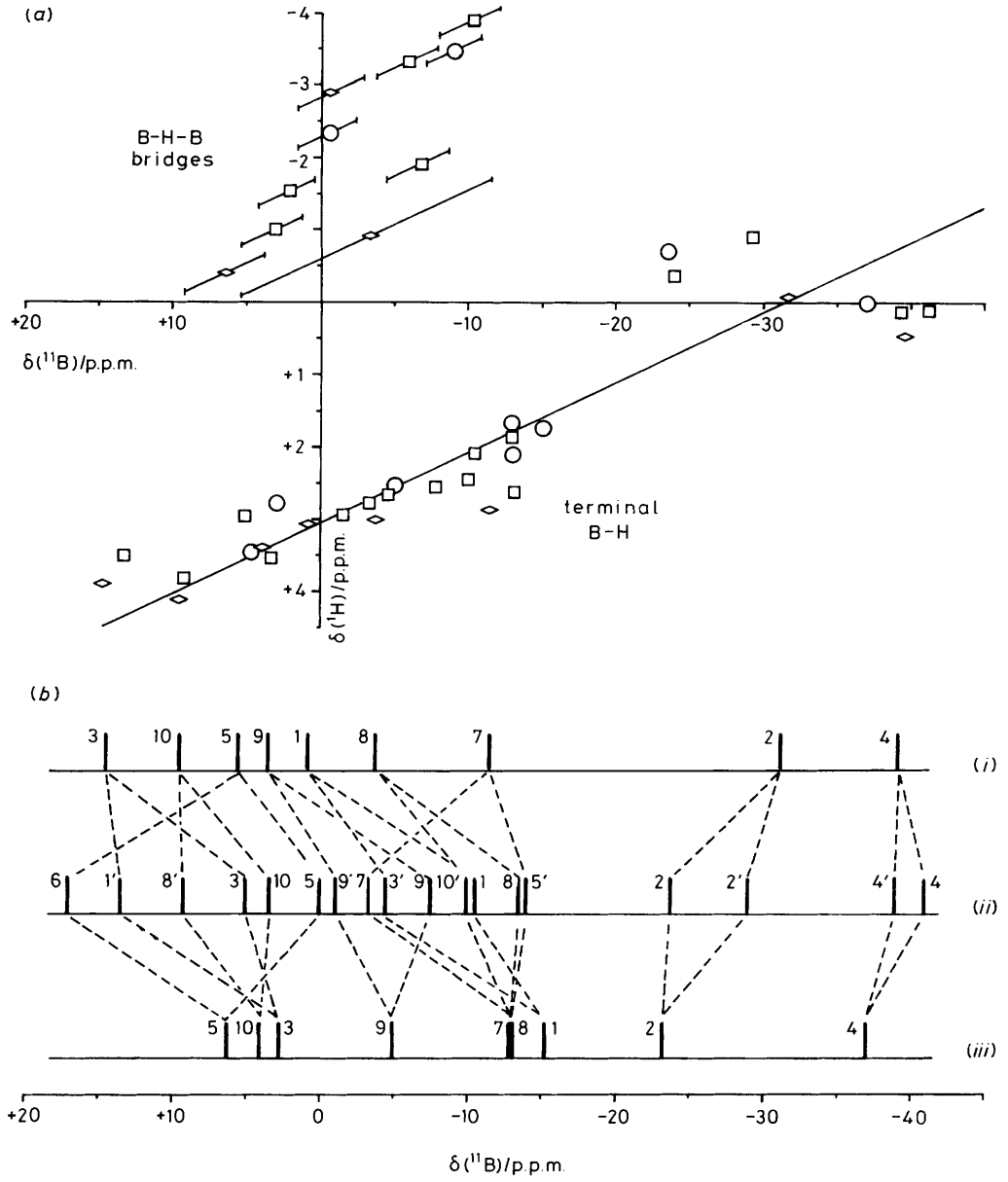

Figure 8. (*a*) A plot of boron-11 *versus* proton nuclear shielding for the hydrogen atoms and their directly bound boron atoms in compounds (**1**) (◇), (**2**) (□), and (**3**) (○). The line drawn has slope $\delta(^1H):\delta(^{11}B) = 1:10$, with intercept $\delta(^1H) = 3.1$ p.p.m. (*b*) Shows the representations of the ^{11}B n.m.r. [same scale as in (*a*)] positions for (*i*) *anti*-$B_{18}H_{22}$ (**1**), (*ii*) *anti*-$[B_{18}H_{21}]^-$ (**2**), and (*iii*) *anti*-$[B_{18}H_{20}]^{2-}$ (**3**)

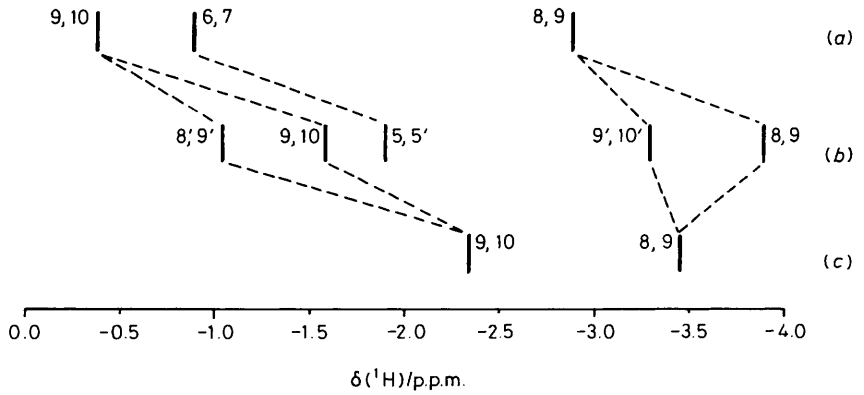

Figure 9. Stick diagram of the proton n.m.r. bridging hydrogen positions for (*a*) *anti*-$B_{18}H_{22}$ (**1**), (*b*) *anti*-$[B_{18}H_{21}]^-$ (**2**), and (*c*) *anti*-$[B_{18}H_{20}]^{2-}$ (**3**)

^1H-$\{^{11}B\}$ and [^{11}B–^{11}B]- and [^1H–^1H]-COSY n.m.r. spectroscopy used were essentially as discussed elsewhere,[8,17–21] other spectroscopy being straightforward. Chemical shifts $\delta(^1H)$ and $\delta(^{11}B)$ are given in p.p.m. to high frequency (low field) of Ξ100 MHz ($SiMe_4$) and Ξ32.083 974 MHz [nominally $BF_3(OEt_2)$ in $CDCl_3$][9] respectively.

Preparation of [1,8-$C_{10}H_6(NMe_2)_2H$][*anti*-$B_{18}H_{21}$].—$B_{18}H_{22}$ (51 mg, 0.24 mmol) and *N,N,N',N'*-tetramethyl-1,8-diaminonaphthalene (55 mg, 0.26 mmol) were stirred in dry, degassed CH_2Cl_2 (20 cm^3) for 24 h. The bright yellow solution was filtered and hexane was added. Bright yellow crystals were deposited on standing (Found: C, 38.65; H, 9.45; B, 45.3; N, 6.35. $C_{14}H_{40}B_{12}N_2$ requires C, 39.0; H, 9.35; B, 45.1; N, 6.50%), m.p. 163—164 °C (with decomposition).

X-*Ray Crystallography*.—Suitable crystals for single-crystal *X*-ray diffraction analysis were obtained by layering an acetone–acetonitrile solution of [NMe_4]$_2$[*anti*-$B_{18}H_{20}$] with diethyl ether.

All crystallographic measurements were made on a Nicolet P3/F diffractometer operating in the ω scan mode using graphite-monochromatized Mo-K_α radiation (λ = 71.069 pm) following a standard procedure described in detail elsewhere.[22] No absorption correction was applied. The structure was solved by direct methods using the SHELX 84 program system[23] and refined by full-matrix least squares using the SHELX 76 program system.[24] All non-hydrogen atoms were assigned anisotropic thermal parameters. Borane hydrogen atoms were readily located in difference Fourier syntheses and were freely refined with individual isotropic thermal parameters. The tetramethylammonium ion was refined as a perfect, rigid tetrahedron pivoting about the nitrogen atom (N–C = 149.3 pm). The cation hydrogen atoms were located in difference syntheses but were fixed as a part of the rigid group with individual isotropic thermal parameters. Carbon–hydrogen bond lengths were in the range 99.1—99.9 pm. The weighting scheme $w = [\sigma^2(F_o) + g(F_o)^2]^{-1}$ was used in which the parameter g was included in refinement in order to obtain satisfactory agreement analyses. Fractional atomic co-ordinates are given in Table 5. Additional material available from the Cambridge Crystallographic Data Centre comprises H-atom co-ordinates, thermal parameters, and remaining bond distances and angles.

Crystal data for [NMe_4]$_2$[*anti*-$B_{18}H_{20}$]. $C_8H_{44}B_{18}N_2$, M = 363.03, monoclinic, a = 693.6(1), b = 1 601.6(3), c = 1 131.6(2) pm, β = 102.07(1)°, U = 1.2237 nm^3, Z = 2, space group $P2_1/c$, D_c = 0.985 g cm^{-3}, μ = 0.21 cm^{-1}, $F(000)$ = 378. Data collection: scans running from 1° below $K_{\alpha 1}$ to 1° above $K_{\alpha 2}$, scan speeds 2.0—29.3° min^{-1}, $4.0 < 2\theta < 45.0°$. 1 671 Unique data collected, 1 523 observed [$I > 1.5\sigma(I)$], T = 290 K.

Structure refinement. Number of parameters = 170, weighting factor g = 0.0002, R = 0.0463, R' = 0.0488.

Acknowledgements

We thank the S.E.R.C. for support and Mr. A. Hedley for microanalyses.

References

1 G. B. Jacobsen, D. G. Meina, J. H. Morris, C. Thompson, S. F. Andrews, D. Reed, A. J. Welch, and D. F. Gaines, *J. Chem. Soc., Dalton Trans.*, 1985, 1645.
2 F. P. Olsen, R. C. Vasavanda, and M. F. Hawthorne, *J. Am. Chem. Soc.*, 1968, **90**, 3946.
3 F. S. Swicker, *Diss. Abstr. Int. B*, 1972, **32**, 4474; L. J. Todd and A. R. Siedle, *Prog. Nucl. Magn. Reson. Spectrosc.*, 1979, **13**, 87.
4 I. J. Colquhoun and W. McFarlane, results presented to the 'First and Third Meetings of British Boron Chemists,' INTRABORON-1, Strathclyde, May 1980, and INTRABORON-3, Leeds, September 1982.
5 T. L. Venable, W. C. Hutton, and R. N. Grimes, *J. Am. Chem. Soc.*, 1982, **104**, 4716; 1984, **106**, 29.
6 J. D. Kennedy, in 'Multinuclear N.M.R.' ed. J. Mason, Plenum, London and New York, 1987, ch. 8, pp. 221—258 and refs. therein.
7 R. F. Sprecher, B. E. Aufderheide, G. W. Luther, and J. C. Carter, *J. Am. Chem. Soc.*, 1974, **96**, 4404.
8 T. C. Gibb and J. D. Kennedy, *J. Chem. Soc., Faraday Trans. 2*, 1982, 525.
9 X. L. R. Fontaine and J. D. Kennedy, *J. Chem. Soc., Chem. Commun.*, 1986, 779.
10 P. G. Simpson and W. N. Lipscomb, *Proc. Natl. Acad. Sci. U.S.A.*, 1962, **48**, 1490.
11 P. G. Simpson and W. N. Lipscomb, *J. Chem. Phys.*, 1963, **39**, 26.
12 See, for example, S. G. Shore, in 'Boron Hydride Chemistry,' ed. E. L. Muetterties, Academic Press, London and New York, 1975, pp. 119—120; J. D. Kennedy, *Prog. Inorg. Chem.*, 1986, **34**, 211.
13 X. L. R. Fontaine, H. Fowkes, N. N. Greenwood, J. D. Kennedy, and M. Thornton-Pett, *J. Chem. Soc., Dalton Trans.*, 1987, 1431.
14 M. Bown, M. A. Beckett, X. L. R. Fontaine, N. N. Greenwood, J. D. Kennedy, and M. Thornton-Pett, *J. Chem. Soc., Dalton Trans.*, 1988, 1969.
15 N. N. Greenwood, J. D. Kennedy, I. Macpherson, and M. Thornton-Pett, *Z. Anorg. Allg. Chem.*, 1986, **540/541**, 45.
16 D. F. Gaines, C. K. Nelson, and G. A. Steehler, *J. Am. Chem. Soc.*, 1984, **104**, 7266.
17 J. D. Kennedy and N. N. Greenwood, *Inorg. Chim. Acta*, 1980, **38**, 93.
18 S. K. Boocock, N. N. Greenwood, M. J. Hails, J. D. Kennedy, and W. S. McDonald, *J. Chem. Soc., Dalton Trans.*, 1981, 1413.
19 S. K. Boocock, J. Bould, N. N. Greenwood, J. D. Kennedy, and W. S. McDonald, *J. Chem. Soc., Dalton Trans.*, 1982, 713.
20 J. D. Kennedy and B. Wrackmeyer, *J. Magn. Reson.*, 1980, **38**, 529.
21 J. D. Kennedy and J. Staves, *Z. Naturforsch., Teil B*, 1979, **34**, 808.
22 A. Modinos and P. Woodward, *J. Chem. Soc., Dalton Trans.*, 1974, 2065.
23 G. M. Sheldrick, SHELX 84 Program System for *X*-Ray Structure Determination, University of Göttingen, 1984.
24 G. M. Sheldrick, SHELX 76 Program System for *X*-Ray Structure Determination, University of Cambridge, 1976.

Received 12*th August* 1987; *Paper* 7/1488